



# Behaviour and material properties of versaloc semi-interlocking mortarless masonry

Sonam Dorji · Hossein Derakhshan · David P. Thambiratnam ·  
Tatheer Zahra · Alireza Mohyeddin

Received: 8 August 2022 / Accepted: 6 January 2023  
© The Author(s) 2023, corrected publication 2023

**Abstract** Masonry construction is popular around the world, but the use of mortared masonry presents numerous challenges. In recent decades, masonry construction systems incorporating interlocking masonry units have been proposed to eliminate mortar. The interlocking between masonry units can be achieved using specially shaped units. This paper presents a comprehensive experimental study to determine the behaviour as well as basic material properties of one such semi-interlocking mortarless masonry. The experiments included testings of ungrouted masonry units, prisms, and wallets. In addition, masonry prisms and wallets with grouted cores were also investigated to study the effect of grouting. A detailed description of the construction

procedure is explained. The failure mechanisms, maximum strengths, force–displacement relationships, and modulus of elasticity of the samples are obtained and contrasted with the relevant results from the literature. Finally, recommendations are made that may assist material model development required for micro- and macro-modelling of mortarless masonry. The new information generated in this research will enable better understanding of the behaviour and properties of semi-interlocking mortarless masonry and will be useful for validating numerical models in future research.

**Keywords** Mortarless masonry · Interlocking masonry · Drystack · Compressive strength · Tensile strength · Modulus of elasticity

---

S. Dorji (✉) · H. Derakhshan · D. P. Thambiratnam ·  
T. Zahra

Faculty of Engineering, Queensland University of  
Technology, Brisbane, QLD 4000, Australia  
e-mail: s5.dorji@hdr.qut.edu.au

H. Derakhshan  
e-mail: hossein.derakhshan@qut.edu.au

D. P. Thambiratnam  
e-mail: d.thambiratnam@qut.edu.au

T. Zahra  
e-mail: t.zahra@qut.edu.au

A. Mohyeddin  
School of Engineering, Edith Cowan University, Perth,  
WA 6027, Australia  
e-mail: a.mohyeddin@ecu.edu.au

## 1 Introduction

Masonry construction is popular around the world, but the use of mortared masonry presents numerous challenges. It is associated with difficulty in quality control, labour-intensiveness, relatively weak brick–mortar bonds, and modelling complexities due to its composite nature [1–3]. For these reasons, research interest has increased in various mortarless masonry systems, especially in the last 20 years [4]. Interlocking mechanisms have commonly been adopted between the masonry units to eliminate the need for



mortar bond. This objective has been achieved by developing specially-shaped units, and the masonry construction made of these units are often interchangeably called mortarless, interlocking, or dry-stacked masonry. This kind of construction can be economical because the ease of alignment reduces the construction costs. According to Ramamurthy & Nambiar [5], the productivity of labour in constructing walls made of mortarless masonry can be increased by as much as 3–5 times.

Structural application of mortarless masonry may be accompanied by grouting, both to enable reinforcement use and to ensure suitable fire performance. However, the use of ungrouted mortarless masonry has also been shown to be a promising application as infill within structural frames [6]. In [6], the use of mortarless masonry as an infill material was found to result in an increased energy dissipation capacity of masonry-infilled frame (MIF) compared to MIF that had mortared masonry.

Despite the above-mentioned mortarless masonry construction advantages, the limitations on its use highlights the need for further research, especially on applicable material modelling techniques such as Concrete Damaged Plasticity model in Abaqus [7]. In view of this requirement, this study was conducted with an objective to characterise mechanical and tensile behaviour properties of mortarless masonry units, prisms and wallets both with and without grout. The research novelty included generating knowledge about mortarless masonry in terms of failure modes, maximum compressive and tensile strengths, force–displacement relationships and compressive modulus of elasticity. To achieve the research objective, a total of 31 tests were conducted on grouted and ungrouted samples. Starting with the literature review, a brief description of the used mortarless masonry units (Versaloc) is explained followed by a report of the experimental study that includes a description of the sample preparation and testing. A discussion of the observed failure patterns is next explained along with a discussion on strengths and force–displacement behaviour. Finally, a potential modelling approach using CDP for mortarless masonry is described.

## 2 Literature review

A review of past experimental investigation shows that ungrouted mortarless masonry compressive strength,  $f_m$ , is typically represented as a ratio of masonry unit compressive strength,  $f_{uc}$ , i.e. ( $f_m/f_{uc}$ ). Tamboo et al. [4] studied 31 different types of interlocking units and found that the  $f_m/f_{uc}$  ratio was 0.45. A similar  $f_m/f_{uc}$  ratio of 0.47 was found in the compressive strength study of interlocking units by Jaafar et al. [8]. These ratios fall outside the range of 0.55 to 0.86, which was suggested by Fortes et al. [9] for 2-stacked mortared but ungrouted concrete masonry prisms. The prisms in that study included mortar with a compressive strength of about 30% of that of the masonry units.

The modulus of elasticity of masonry material is generally calculated as a product of a scalar coefficient and compressive strength (ASCE 41–17 [10]) which is represented by  $E_{uc}/f_{uc}$ ,  $E_m/f_m$  and  $E_{mg}/f_{mg}$  ratios, respectively, for masonry units, ungrouted prisms and grouted prisms. The value of  $E_m/f_m$  ratio has been widely studied for mortared masonry. The Australian Masonry Standard AS 3700 [11] recommends the mortared masonry  $E_m/f_m$  ratio to be 700 for short-term loading. Similarly, a ratio of 1000, 850 and 1000 has been suggested for mortared masonry, respectively, in Eurocode 6 [12], Canadian masonry code [13], and Paulay & Priestly [14]. Contrarily, there are no such recommendations made for mortarless masonry.

The above discussion highlights the differences between the compressive behaviour of mortared and mortarless masonry and the limitation in the literature on the mortarless masonry material properties. In addition, it is hypothesised that the damage pattern under compression forces be different from that of mortared masonry. While some experimental evidence is available [8] which suggests both mortarless masonry units and 3-stack prisms when subjected to compression, fail by cracking at the intersection of the face- and web- shells, the scope of the data is limited. In contrast, in the testings of mortared but ungrouted concrete prisms, Huang et al. [15] observed that vertical cracks developed at the face-shell which propagated throughout the height of the prism in a brittle failure.

Similarly, it is hypothesised that the effects of grouting on mortarless masonry be different from that in mortared masonry. Grouting has been found by Jaafar et al. [16] to increase the compressive strength and stiffness of mortarless masonry prisms, even though the used grout had a compressive strength,  $f_{cg}$ , equal to 87.2% of the  $f_{uc}$ . This pattern is consistent with observations for mortared masonry by Bolhasani, et al. [17], who suggested a high-strength grout increases masonry prism strength. However, these findings lack generality because recent research by Martins et al. [18] demonstrated that the effect of grouting in mortared masonry is still controversial.

In comparison to the compressive material behaviour investigations cited above, there is no documented study on the tensile properties of ungrouted or grouted mortarless masonry wallets. Therefore, the tensile strength of masonry unit,  $f_{tu}$ , is generally assumed to be 10% of the compressive strength of the units in the Finite Element (FE) models in the recent studies of Shi et al. [19], Zahra [20] and Martínez et al. [21]. One of the techniques to measure the tensile strength of mortared masonry composite is to conduct diagonal tension test, which entails subjecting masonry wallets to diagonally compressive loads [22–27]. As the joints in ungrouted mortarless masonry are dry and susceptible to in-plane sliding, the feasibility of conducting diagonal tension test on this type of construction was studied in the present investigation.

In summary, the above review suggests that while mortared masonry material property has been studied well, establishing relationships between various properties of interlocking masonry systems requires further research. In view of this shortcoming, this research program was developed to study relationships between various material properties of a certain type of interlocking masonry system called Versaloc. It is highlighted that various other interlocking masonry systems are also available, each requiring separate investigations. The research scope is limited to experimental investigation, and therefore finite element modelling is excluded from this report.

## 2.1 Versaloc units

Most current application of ‘modern’ mortarless masonry is in developed countries such as Australia,

where several types of suitable masonry units are available in the market. One of the masonry unit types is Versaloc (Fig. 1), which is manufactured by Adbri Masonry [28] under the umbrella of Concrete Masonry Association of Australia (CMAA). A typical mix design of the masonry units constitutes 11% cement, 70% sand, 8% aggregate (7 mm) and 1% slag [28]. These masonry units have different types suitable for different locations within the wall, with the end- and half-units that are shown in being course starters while the standard-units being used elsewhere. An approximate schematic diagram of the standard-unit is illustrated in d, and a detailed geometrical description of the unit can be found in Dyson [29]. The required interlocking occurs due to the lugs located on top and the tongue-and-groove (T&G) system located at the ends of the unit (a). However, the units are called semi-interlocking mortarless products because the aforementioned lugs and T&G restrain the movements only in the out-of-plane wall direction. The large cores in the units allow for reinforced wall construction and can also be grouted. According to the annual report of Adelaide Brighton Ltd. [30], the introduction of these Versaloc units has been rapidly accepted in certain construction markets, but research is required into material properties and numerical modelling strategies for wider application.

## 3 Construction of test specimens

In addition to grout cylinders, the test specimens included a set of ungrouted masonry units, prisms, and wallets, and another set with grouted masonry prisms and wallets. The physical properties of the mortarless masonry units used in this study are being listed in Table 1. The density of the units was measured by dividing the weight (in kg) of one masonry unit by its solid volume and was found to be slightly greater than 2200 kg/m<sup>3</sup>. The bearing area listed in Table 1 is a ‘nominal’ area that is equal to the product of the masonry unit length and the sum of the masonry unit shell thicknesses, which was measured to be, on average, 32.2 mm. The end- and standard-units were similar except that the former had one additional web shell at the end which resulted in higher nominal bearing area than the latter (see Table 1). As discussed later, only a part of the face-shell thickness had

**Fig. 1** Types of 150 mm thick Versaloc masonry units

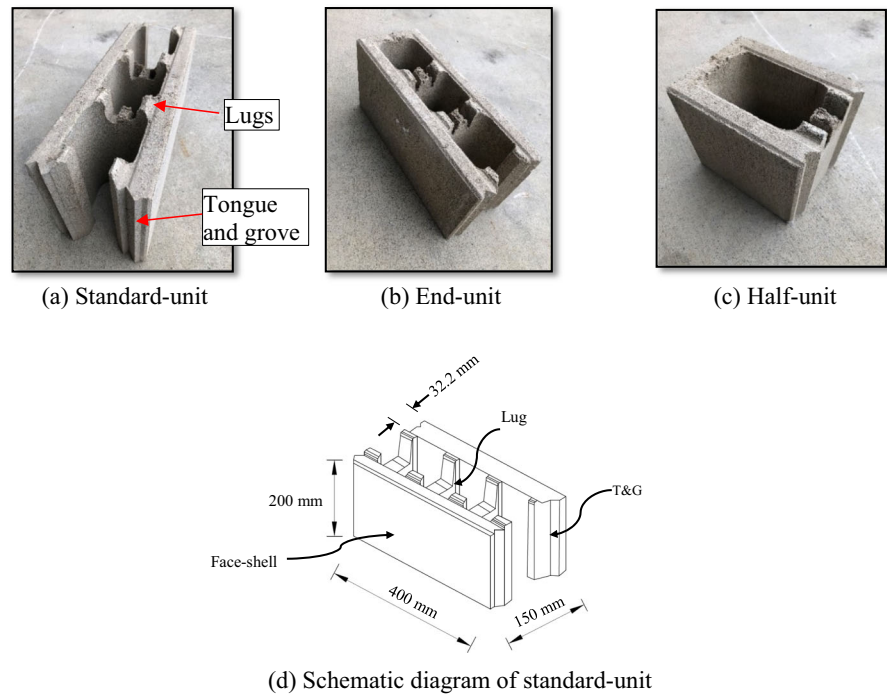


**Table 1** Properties of Versaloc masonry units

Type of unit	Dimensions (mm)			Solid-to-gross volume ratio	Weight (kg)	Density (kg/m <sup>3</sup> )	Bearing area (mm <sup>2</sup> )
	Length	Height	Width				
Standard	400	200	150	0.51	13.5	2206	25,760
End	400	200	150	0.55	14.6	2212	37,975
Half	200	200	150	0.56	7.4	2202	12,990

participated in taking the compressive loads due to the end of the shell being tapered.

Due to no specific standards being available for construction and testing mortarless masonry, the relevant standards of mortared masonry were followed as summarised in Table 2. The prisms were two-stack (nominal length  $\times$  height  $\times$  thickness dimensions of 400  $\times$  400  $\times$  150 mm) and constructed using the standard-units (see Table 2) following ASTM C1314-21 [31]. During the construction of grouted specimens, formwork was provided all around the specimens to assist with grouting. The bottom unit was first laid, poured with grout and then compaction using metal rods followed by the placing of the top unit. The grouted prisms were cured for at least 28 days before being transported for testing.

The size of the ungrouted wallets was 1200  $\times$  1200  $\times$  150 mm as per the minimum dimensions recommended by ASTM E519/E519M—21 [34]. They were constructed by placing one end-unit on a levelled platform at the same location where the test set-up discussed in Sect. 0 was performed. Next, a standard-unit was placed ensuring that the end-unit and the standard-unit interlocked followed by the placing of the other end-unit to complete the course. The level on top of the first course was checked before proceeding to the second course. The corner half-unit of the second course was then laid ensuring horizontal and vertical alignments with respect to the course below. The second course was completed using two standard-units and an additional half-unit at the other end that ensured that staggered vertical joints were

**Table 2** Test specimens

Material property	Number of samples	Size of sample (mm) (length × height × thickness)	Standard
Compression of ungrouted masonry unit, $f_{uc}$	5	400 × 200 × 150	ASTM C140/C140M—21 [32]
Splitting tensile strength of ungrouted masonry unit, $f_{tu}$	5	400 × 200 × 150	ASTM C1006/C1006M—20 [33]
Compression of ungrouted masonry prism, $f_m$	4	400 × 400 × 150	ASTM C1314—21 [31]
Compression of grouted masonry prism, $f_{mg}$	4	400 × 400 × 150	ASTM C1314—21 [31]
Diagonal tension of ungrouted masonry wallet, $f_{tu}$	4	1200 × 1200 × 150	ASTM E519/E519M—21 [34]
Diagonal tension of grouted masonry wallet, $f_{tg}$	3	1200 × 1200 × 150	ASTM E519/E519M—21 [34]
Compression of grout cylinder, $f_{cg}$	3	100 dia × 200 high	ASTM C39/C39M – 21 [35]
Splitting tensile strength of grout cylinder, $f_{ct,f}$	3	100 dia × 200 high	ASTM C496/496 M—17 [36]

obtained. The procedure was repeated for all other courses, except that in laying the sixth course, the lugs from the units were removed to ensure a flat top surface.

The same procedure was followed for the grouted samples, but for convenience they were constructed away from test set-up location. Grouting was done after laying all masonry units in each course and then compacted using rods. The same batch of grout was used to prepare grouted prisms, wallets, in addition to six grout cylinders (100 × 200 mm high). All samples were constructed by the research team with occasional helps from the lab technicians. Similar to grouted prisms and grout cylinders, the grouted wallets were cured for 28 days before lifting and transporting to the test set-up location.

#### 4 Test set-ups

Since the testing procedure of grout cylinders are well established, they are avoided from discussions, and that only the ones related to mortarless masonry are explained here. A 2000 kN INSTRON machine was used to apply the compressive load in the test set-up (Fig. 2a) of the masonry unit following the ASTM C140/C14—21 [32] standard. The machine was integrated with a computer to record the applied force

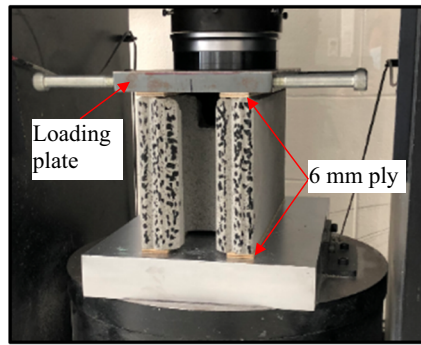
and the displacement of the sample at a user-defined interval which was set up as 1 mm/minute for all samples. Before the samples were placed in the set-up, the lugs were removed and a 400 mm × 35 mm × 6 mm ply was placed on top and bottom of each face-shell. A steel plate was placed on top to transfer the applied forces to the masonry unit.

The Brazilian splitting tensile test was performed as per ASTM C1006/C1006M—20 [33] to obtain the tensile strength of the masonry unit (see Fig. 2b) using the same machine discussed above. A steel plate was positioned at the bottom and top of the sample. The splitting tensile load on the unit was applied through the 16 mm × 16 mm plys placed at the bottom and top of the unit that had marked points to minimise eccentricity of loading.

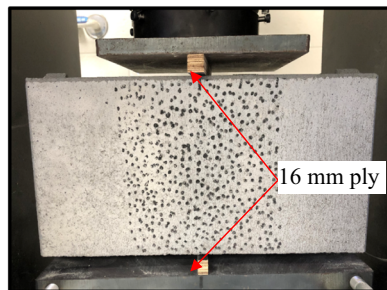
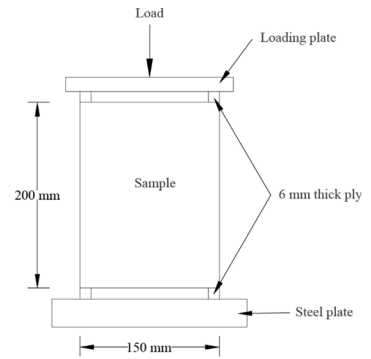
The set-up (see Fig. 2c) for the ungrouted and grouted prism testing was done using ASTM C1314—21 [31] for which a machine with a 4000 kN capacity was used that was also equipped to measure both force and displacement. Similar to the procedure for the masonry units, plys were placed at the bottom and top of the prisms, and a loading rate of 1 mm/minute was applied.

To measure masonry wallet tensile strength, ASTM E519/E519M—21 [34] was used to conduct diagonal tension tests. The test set-up procedure was same in both ungrouted and grouted wallets except that the

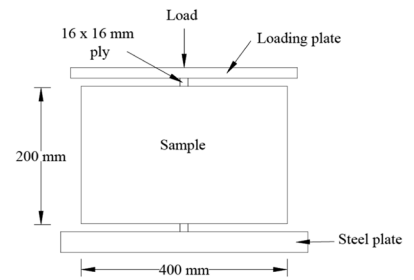
Fig. 2 Test set-ups



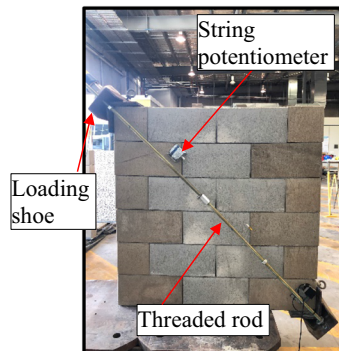
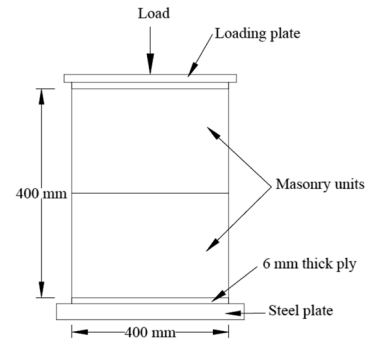
(a) Masonry units - Compression



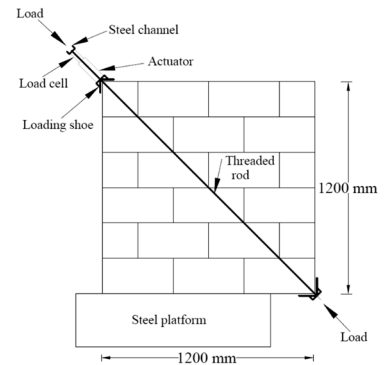
(b) Masonry units - Tension



(c) Prisms - Compression



(d) Wallets - Diagonal tension



latter had to be transported to the test set-up area using slings. Loading shoes of  $250 \times 300 \times 6$  mm were first set-up at the two opposite corner ends of the wallets (see Fig. 2d). The load was applied by means of two high-tensile 20 mm threaded rods that were connected to an actuator with a 500 kN capacity with manual operation. The applied load was measured by a load cell, while the deformations were measured using string potentiometer as shown in Fig. 2d. It is highlighted that masonry failure in diagonal tension test is limited to combined effects of compression and shear stresses. Masonry material failure under pure tension, and combined tension and shear stresses were not investigated in this study and are recommended in future research.

## 5 Failure patterns

### 5.1 Masonry units

There was hardly any visible deformation prior to failure in the masonry units. At failure (average load of 622.87 kN), there was a sudden large crack from the outside of both face-shells. As a result, a part of the face shell was delaminated, and this observation was consistently made in all samples (see Fig. 3a). A closer inspection after the test samples showed that the face-shell had also cracked on the inside between the webs (see Fig. 3a) in a similar manner resembling the failure

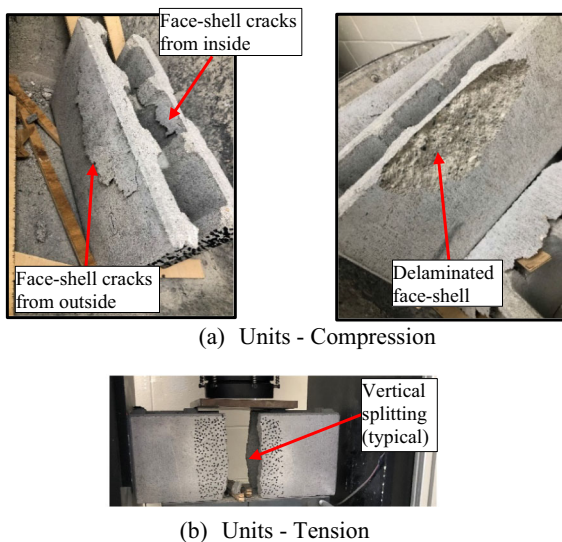


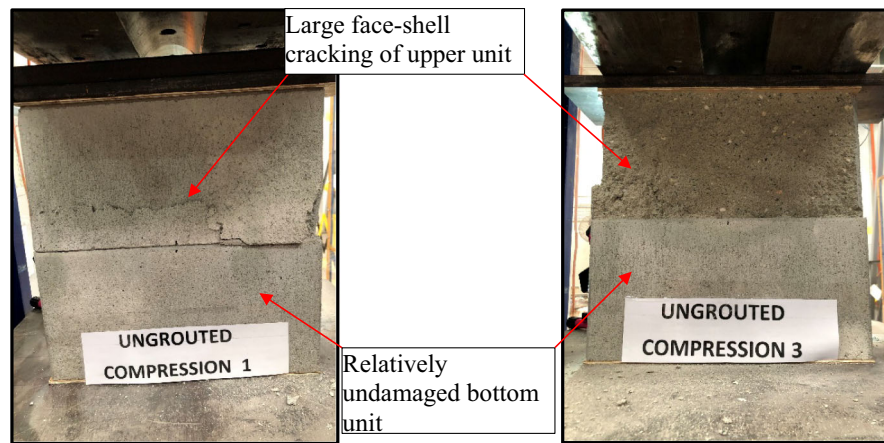
**Fig. 3** Typical failure modes of masonry units

mode observed in Jaafar et al. [8]. The typical mode of failure (see Fig. 3b) in the splitting tensile test of the units included almost vertical splitting of the unit at the maximum load which was observed to be 53.14 kN on average. Similar to compression, no noticeable damage occurred before the maximum load was reached.

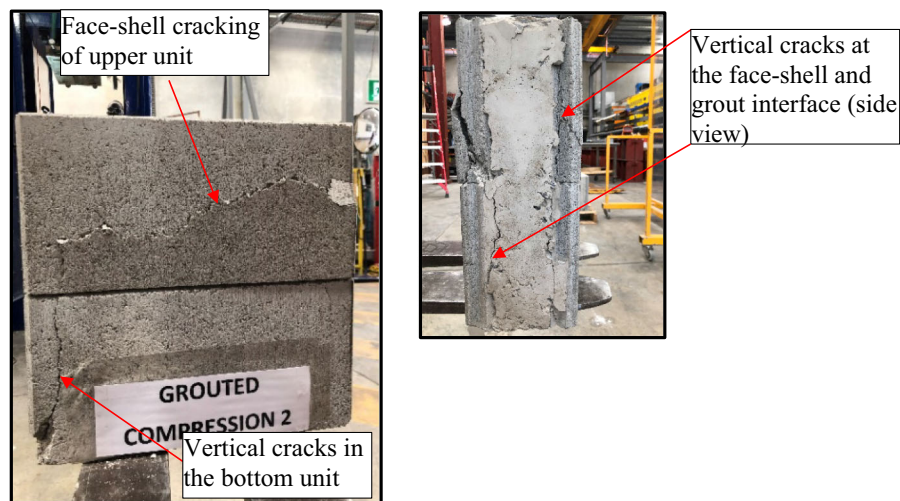
### 5.2 Masonry prisms

Except for one sample that is discussed later, other ungrouted prism samples failed due to spalling of the face-shell of the top masonry unit (see Fig. 4a) at the maximum strength (average load of 314.34 kN), similar to the failure mode observed for masonry units. The spalling was followed by the slippage between the two units at the joint. The exception was one of the samples, in which the slippage was very pronounced and resulted in the top unit to move in the out-of-plane direction by about 3.6 mm relative to the lower unit. It was also observed that the upper unit had suffered more damage than the lower unit, which was almost intact (see Fig. 4a). This observation is in contrast with damage pattern reported in the literature for mortared concrete masonry (e.g. Huang et al. [15] as discussed earlier), which included cracking through the full prism height. This difference in crack patterns indicates that compression cracking in larger construction of mortarless masonry may also be different from that observed for mortared masonry. For safety reasons and to prevent damage to the test set-up, testing of the ungrouted samples were stopped when the slippage became visible.

In contrast to the above observations of ungrouted prisms, grouted prisms failed due to cracks that propagated through both units (Fig. 4b) at maximum strength which occurred at 733.71 kN on average. In addition, no slippage between the two units were observed in the samples. Cracks were also found at the interface of the grout and the face-shell (Fig. 4b), that can be attributed to the difference in the strength properties of the grout (6.23 MPa) and the unit (40.98 MPa). With these properties, the masonry units are assumed to be stiffer than the grout, and the difference in the stiffness resulted in shear cracking of the interface between the two materials.



(a) UngROUTed prisms - Compression



(b) Grouted prisms - Compression

**Fig. 4** Typical failure modes of masonry prisms

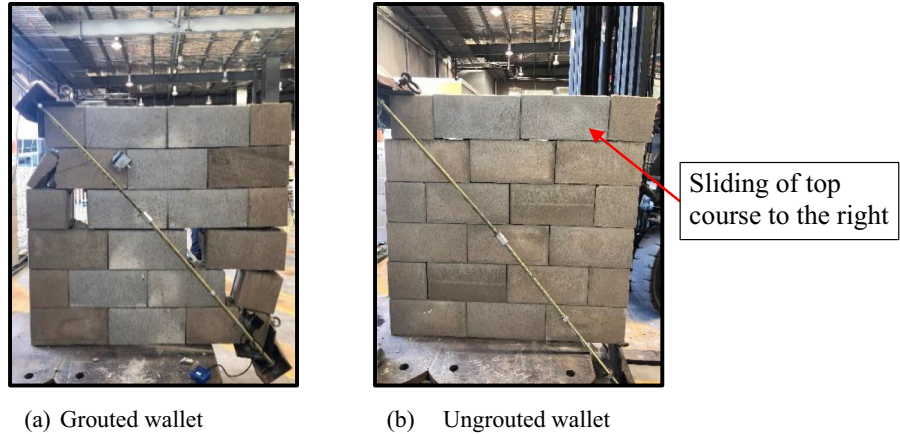
### 5.3 Masonry wallets

For grouted wallets, the load was gradually increased until the wallets failed in shear. There were no visible cracks before the wallets suddenly failed at maximum load (average load of 133.67 kN) as shown in Fig. 5a. The failure consisted of stepped cracking, which included flexural tension cracks in the perpend near the loading shoes and shear sliding in several courses similar to the findings common for mortared masonry (e.g. Dizhur and Ingham [23]). The masonry units along the other diagonal were relatively undamaged. The instrumentation set-up for measuring displacement had some technical issues, and therefore only the strengths of the grouted wallet are reported herein.

In the case of ungrouted wallets, the wallets developed immature sliding at the top course (Fig. 5b) with a stepped-separation of the masonry along the joint at a relatively small force of 4 kN. This repeatedly observed failure pattern can be considered as governing the in-plane behaviour for wallet aspect (height-to-length) ratios less than 1. For this reason, the standard interpretation of the diagonal tension test results as presented in the literature [22–27] is not applicable to these wallets.



**Fig. 5** Typical failure modes of wallets in tension



(a) Grouted wallet

(b) UngROUTED wallet

## 6 Analysis of results and discussion

### 6.1 Compressive strength

The compressive strength given in Eq. (1) was used to calculate  $f_{uc}$ ,  $f_m$ ,  $f_{mg}$ , and  $f_{cg}$ , with the results being presented in Table 3.

$$f = \frac{F}{A} \quad (1)$$

In Eq. (1),  $f$  represents compressive strength,  $F$  is the applied maximum force and  $A$  is the cross-sectional area. In the case of masonry unit and ungrouted prism,  $A$  was determined using the depressed area of the levelling plys that were placed between the loading platen and the sample. This area was smaller than the nominal face-shell area as the width of the depression was, on average, 19 mm (see Fig. 6), which is less than the measured average face-shell thickness of 32.2 mm as discussed earlier. This observation indicates that only partial thickness of the



**Fig. 6** Impression on ply caused by the application of compressive loads

face-shell participated in taking loads when subjected to compressive force. For grouted prisms, the full unit thickness of 150 mm was considered as the load was applied both to the grout and the masonry unit.

**Table 3** Compressive strengths

Type of testing	Number of samples	Average maximum load (kN)	Average compressive strength in MPa (COV)	Average strain at maximum compressive strength ( $10^{-3}$ )
Masonry unit	5	622.87	40.98 (5.7%)	1.15
UngROUTED prism	4	314.34	20.68 (17.2%)	2.81
Grouted prism	4	733.71	12.21 (5.7%)	2.01
Grout	3	48.90	6.23 (19.4%)	1.01

The average masonry unit strength,  $f_{uc}$ , was found to be 40.98 MPa as shown in Table 3 with a Coefficient of Variation (CoV) of 5.37% against the manufacturer's supplied strength of 20 MPa [28]. Conversely, the ungrouted prism strength,  $f_m$ , was calculated as, on average, 20.68 MPa, which is significantly lower than  $f_{uc}$ . Therefore, a relationship between the two values can be established as shown in Eq. (2), which is consistent with the findings of Thamboo et al. [4] and Jaafar et al. [8] discussed earlier. It is highlighted that the masonry units in the current research was substantially stronger than those reported in Thamboo et al. [4], and therefore the relationship of Eq. (2) appears to have a wide application range.

$$f_m = 0.51f_{uc} \quad (2)$$

where  $f_m$  and  $f_{uc}$  are the average compressive strengths of the ungrouted prism and the unit respectively. The reasons for  $f_m$  being smaller than  $f_{uc}$  is attributed to the well-documented effect of the presence of joint between the units and the increase in slenderness ratio [11, 37].

The influence of grouting on  $f_m$  was found to be substantial when calculated using gross area (see Table 3), where the compressive strength of the grouted prism has decreased by 41.0% compared to the compressive strength of ungrouted prisms. The significant reduction in the strength is attributed to the increase in the cross-sectional area of grouted prisms which included 150 mm masonry thickness compared to 38 mm in ungrouted prisms. Another reason was due to the use of the relatively low-strength grout to fill the masonry cores. This reasoning is evidenced from the finding of Bolhassani et al. [17] which found that when the compressive strength of the grout was higher than that of the unit, the resultant strength of grouted prism was observed to be greater than that of the ungrouted prism strength. Although the strength has decreased in this study, grouting substantially increased the maximum load carrying capacity of the prism. The average load capacity of the five grouted prism samples was 733.71 kN (see Table 3) which is an increase of 102.0% compared to the sum of the average load capacities of ungrouted prisms and grout that corresponded to 363.24 kN. A relatively higher COV was obtained for the grouted masonry prism and grout cylinder compression tests as shown in Table 3. The reason for the unusually high COV was attributed

to the small number of samples tested. Although the number of samples complies with the minimum requirements set in the Australian Masonry Standard AS 3700 [11], it is recommended that a greater number of samples be tested in any future investigations.

## 6.2 Tensile strength

Both ASTM C1006/C1006M—20 [33] for masonry unit and ASTM C496/496 M—17 [36] for concrete material use the formula given in Eq. (3) to estimate their respective splitting tensile strengths:

$$f_{ct.sp} = \frac{2P}{\pi AB_n} \quad (3)$$

where  $f_{ct.sp}$  is the splitting tensile strength and  $P$  is the maximum applied load.  $A$  is either the cylinder diameter or the masonry unit height, and  $B_n$  is either the cylinder height or the sum of the face-shell thicknesses of the masonry unit (equal to 38 mm). The tensile strengths of both cylinder,  $f_{ct}$ , and the masonry unit,  $f_{ut}$ , were estimated as 85% of their corresponding splitting tensile strengths as per Balbo [38].

In the case of grouted masonry wallets, the tensile strength of masonry wallet is estimated following ASTM E519/E519M—21 [34] using Eq. (4) as:

$$f_{ig} = \frac{0.707P}{A_n} \quad (4)$$

where  $f_{ig}$  is the grouted wallet tensile strength,  $P$  is the maximum load applied and  $A_n$  is the net area of the sample given by:

$$A_n = \left(\frac{w+h}{2}\right)tn \quad (5)$$

In Eq. (5),  $w$ ,  $h$  and  $t$  are, respectively, the width, height and thickness of the wallets and  $n$  is the percent of gross area of the unit that is solid and hence  $n$  equals one for grouted cores.

Alternatively, the ASCE 41–17 [10] guideline recommends the estimation of tensile strength of masonry wallets as given in Eq. (6).

$$V_{dr} = f_{ig} \frac{wh}{b} \sqrt{1 + \frac{f_d}{f_{ig}}} \quad (6)$$

In Eq. (6),  $V_{dr}$  is the lateral strength,  $f_{ig}$  is the masonry tensile strength,  $w$  and  $h$  are the width and height of the wallet,  $b$  is 0.67 for  $w/h < 0.67$ ,  $w/h$



when  $0.67 \geq w/h \leq 1.0$ , and 1.0 when  $w/h > 1.0$ , and  $f_d$  is the axial compression stress. In calculating  $f_d$ , axial forces include the vertical component of the diagonally applied force and the self-weight of the wall which has been assumed at mid-height in this study. Since  $V_{dt}$  is known from the experimental testing as the horizontal component of the diagonally applied compressive force,  $f_{dg}$  can be estimated as illustrated in Eq. (4).

Both Eqs. (4) and (6) were used to calculate grouted tensile strengths, which are listed in .

Table 4 along with tensile strengths of masonry units and grout. The average grouted tensile strength was found to be 0.53 MPa and 0.55 MPa, respectively from Eqs. (4) and (6) highlighting the good agreement between ASCE 41–17 [10] and ASTM E519/E519M–21 [34].

A comparison of the tensile strengths of the masonry unit, grouted wallets and the grout is given in Table 4. It is seen that the average tensile strength of the grouted wallet is considerably lesser than the tensile strength of the masonry unit. Instead, the grouted wallets tensile strength is comparable to grout tensile strength, which was 0.53 MPa. This comparison indicates that the wallets failed when the stress reached the grout tensile strength. The ratio of the tensile strength to compressive strength was found to be 9.2% and 4.3%, respectively, for masonry units and grouted wallets. These results indicate that the commonly assumed 10% ratio in the literature as explained earlier can be an overestimation of the masonry tensile strength.

It was found in this research that the application of Eq. (4) can be limited only to grouted wallets, with the reason being that all four ungrouted samples unanimously underwent sliding at the top course. The sliding meant that the loading condition of these calculations (diagonal) was not continually met. Therefore, it is recommended based on the results to

assume the bed-joint shear strength as the tensile strength of masonry composite in the case of ungrouted mortarless construction. This suggestion has been mentioned by ASCE 41–17 [10] as being a conservative estimate for mortared masonry.

As discussed in the Introduction, the application of ungrouted mortarless construction may be most relevant in the construction of MIFs. For macro-modelling of such structures, the infill panel can be assumed to have a tensile strength calculated as the product of coefficient of friction,  $\mu$ , by the axial stress,  $f_d$ , at the panel mid-height. The coefficient of friction can be assumed as 0.75 for interlocking masonry according to Hossain et al. [39]. Based on this recommendation and using the axial stress (due to self-weight only) at the wallet mid-height of 0.016 MPa, the estimated tensile strength of ungrouted mortarless masonry wallets is  $(0.75 \times 0.016 =) 0.012$  MPa for all samples.

### 6.3 Stress–strain relationship

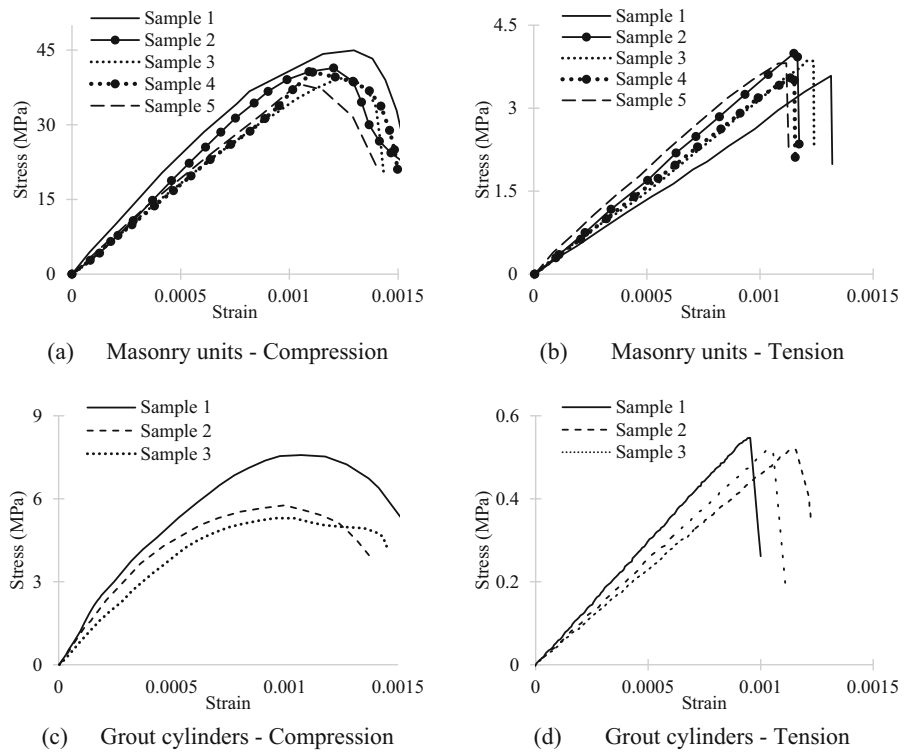
To construct stress–strain curves, strains were calculated by dividing the recorded displacement from the machine by the original height of the specimen. The height of masonry units, grout cylinders, ungrouted prisms, and grouted prisms was assumed as 200 mm, 200 mm, 400 mm and 400 mm respectively. As each curve included an initial nonlinear ‘settling’ portion, that included initial strain (but not the stress) was removed from calculations.

The compressive stress–strain curves of the masonry units are shown in Fig. 7a, which show an approximately linear relationship before the maximum strength is reached. The softening branch of the stress–strain curve was observed to be relatively steep (i.e. rapid decrease in post-peak strength). Figure 7b illustrates that the tensile response of the masonry units was approximately linear up to the point of maximum strength. At failure, the strength suddenly

**Table 4** Tensile strengths

Type of testing	Number of samples	Average maximum load (kN)	Tensile strength in MPa, (COV)	
Grouted wallet	3	133.67	From Eq. (4) 0.53 (19.9%)	From Eq. (6) 0.55 (19.9%)
Unit	5	53.14	3.78 (5.1%)	
Grout	3	19.47	0.53 (3.6%)	

**Fig. 7** Stress–strain relationships of masonry units and grout cylinders

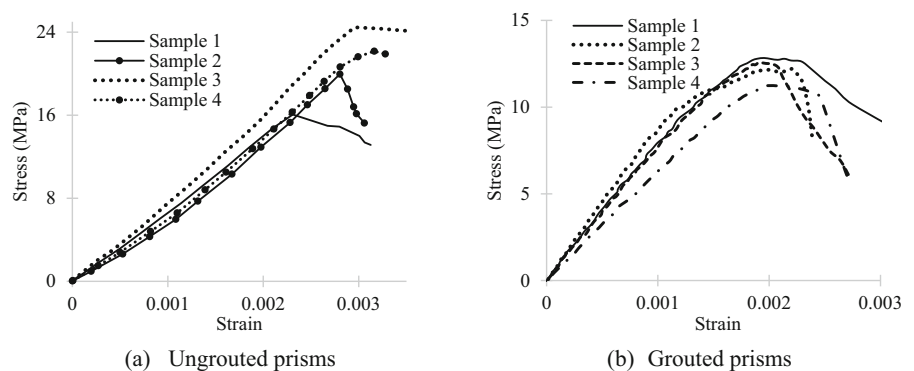


dropped without any increase in strain. The grout cylinders exhibited a slightly more nonlinear compressive behaviour compared to that of the masonry units as shown in Fig. 7c. Conversely, the grout tensile behaviour was linear (Fig. 7d) followed by brittle cracking as was the case for masonry unit due to same method of testing (i.e. splitting test) being used in both of them.

The stress–strain curves for ungrouted prisms are shown in Fig. 8a which shows an initially less stiff branch with some nonlinearity compared to the linear and stiff relationships observed in the masonry units.

This phenomenon is attributed to the presence of a dry joint between the masonry units in ungrouted prisms, which required closing-up before the maximum strength was reached. Once the maximum strength has been achieved, the ungrouted samples exhibited different softening behaviours due to the slippage of the top masonry unit with respect to the bottom unit as explained earlier in the discussion of failure patterns. The average strain at maximum strength,  $\epsilon_{0m}$ , for ungrouted prisms is found to be 0.00281 (see Table 3), which is 144.3% higher than that for masonry units

**Fig. 8** Compressive stress–strain relationship for ungrouted and grouted prisms



(0.00115) confirming the less stiff behaviour of ungrouted prism discussed above.

The compressive behaviour of the grouted prisms up to the maximum strength is similar to that of the masonry units showing approximately linear relationship (see Fig. 8b). However, compared to the masonry units that had an average  $\varepsilon_{0m}$  of 0.00115, the corresponding  $\varepsilon_{0m}$  for the grouted prisms was 0.00201 which is 74.8% larger than that of the masonry units (see Table 3). The finding is attributed to the higher slenderness ratio of grouted prisms and to the presence of the low-stiffness grout in the composite structure of the grouted samples. The effect of low-stiffness grout is further evidenced by the fact that due to the absence of grout in ungrouted samples,  $\varepsilon_{0m}$  was 39.8% higher at 0.00281 than that of the grouted samples. For the same reasons of higher slenderness ratio and the presence of less stiff grout, the softening branch of grouted prisms, except for sample 2, was found to be less steep in comparison to that of the masonry units. The average strain at maximum strength,  $\varepsilon_{0m}$ , of the grouted prisms at maximum strength is 99.0% greater than that of the grout cylinder (0.00201 for grouted prisms against 0.00101 for grout cylinders; see Table 3).

Following the ASCE 41–17 [10] guideline, the modulus of elasticity of the tested samples was estimated as the slope between the points at 5% and 33% of the maximum strength. From Table 5, it can be seen that the average modulus of elasticity of two-stack ungrouted masonry prism,  $E_m$ , (6558.16 MPa) is 14.9% of the modulus of elasticity of masonry units,  $E_u$ , (43,996.71 MPa). The  $E_u/f_{uc}$  ratio of the masonry units is measured to be 1073.61 MPa comparing well with the finding of Martínez & Atamturkur [40] but substantially higher than that observed in Shi et al. [19]. In the case of ungrouted prisms, the  $E_m/f_m$  ratio corresponds to 317.12 which is significantly lower than the typical range of ratios for mortared masonry discussed in the Introduction. The smaller ratio for mortarless masonry is attributed to the lack of

presence of a mortar that can effectively bond the units together. Instead, the ungrouted prisms included dry joints that can undergo substantial deformation under the applied compression.

For grouted prisms, the modulus of elasticity,  $E_{mg}$ , is found to be 7842.25 MPa which is 19.6% higher than that of the ungrouted prism, and the  $E_{mg}/f_{mg}$  ratio is approximately 642.28 which is still lesser than the typical recommendations for mortared masonry. Compared to grouted prisms, the modulus of elasticity of grout cylinders,  $E_{cg}$ , is 45.0% higher which occurred due to the cylinders failing at much lower strains. However, the finding related to grouted prism is from only one strength of grout, and a much higher number of investigations are necessary to completely understand the effect of grouting on the material properties of mortarless masonry.

## 7 Potential modelling approach for material modelling

As discussed in Introduction, the material properties characterisation is required for modelling techniques, and a potential modelling approach using CDP in Abaqus [7] is described in this section. CDP is a continuum, plasticity-based, damage model which has commonly been applied in both micro-scale and macro-scale modelling studies. In micro-modelling approach, the masonry units and the joints are modelled separately, requiring the material properties of the masonry units. Some of the recent micro-scale studies on mortarless masonry modelling include Shi et al. [19], Zahra [20] and Martínez et al. [21]. In macro-modelling, the whole masonry can be considered as one homogeneous material, with masonry prism material properties being required. The CDP model assumes the response of the material to be initially elastic, followed by a plastic behaviour. In the elastic definition, the modulus of elasticity,  $E$ , and Poisson's ratio,  $\nu$ , are required. While  $E$  can be used from that obtained from the experimental testing for different materials discussed earlier,  $\nu$  can be adopted from literature such as 0.2 for both concrete and masonry [41].

The plastic response needs compressive stress-crushing strains and tensile stress-cracking strain behaviours. To establish the crushing strains in

**Table 5** Modulus of elasticity (MPa)

$E_u$	$E_m$	$E_{mg}$	$E_{cg}$
43,996.71	6558.16	7842.25	11,370.98

compression, the material yield point is required which is suggested at 60% of the maximum strength in Zahra [42]. Crushing strains are then calculated for the yield point and beyond as total strain minus the strain at yield point. Therefore, the crushing strain at yield point becomes zero as shown in Table 6. The process is similar in calculating the cracking strain in tension; however, the yield point is required to be considered at maximum tensile strength in the model. As discussed earlier, there was no softening branch in the tensile behaviour of the masonry units, and therefore the point at maximum strength on the force–displacement curve (or yield point) can be considered as the cracking strain data (Table 7). While a similar recommendation has been proposed for ungrouted and grouted constructions, the ungrouted mortarless masonry tensile strength can be assumed as equal to coefficient of friction,  $\mu$ , times the axial stress,  $f_d$ , at wall mid-height (see Table 7) as discussed earlier.

## 8 Conclusions

A total of 31 tests were conducted to characterise the compressive and tensile behaviours of mortarless masonry units in addition to the various properties of prisms and wallets that were built using semi-interlocking mortarless masonry units both with and without grout. The tests were performed using the relevant standards of mortared masonry.

The absence of mortar joint in the masonry prisms resulted in the reduction of compressive strength (20.68 MPa) by almost half compared to that of the masonry units (40.98 MPa). When calculated on gross area, grouting of masonry unit cores of grouted prisms with low strength grout led to a decrease in strength by 41.0% in relation to the compressive strength of ungrouted prisms.

The ungrouted prism samples failed by face-shell cracking of the top unit and slippage between the two masonry units. Unlike in mortared masonry, no damage was observed in the bottom unit due to the lack of mortar for the cracks to propagate through the joints which indicated that compression cracking in larger construction of mortarless masonry can differ from that of the mortared masonry. Contrary to ungrouted prisms, the presence of grout in grouted prisms resulted in the development of cracks in both top and bottom masonry units.

The stress–strain behaviour of ungrouted prisms was relatively less stiff compared to that of the masonry units and the grouted prisms. This phenomenon was attributed to the failure mode observed for mortarless masonry prisms where the absence of material between the top and the bottom unit led to the latter being relatively undamaged in the testing.

Tensile strengths of masonry units (3.78 MPa) and grouted wallets (0.53 MPa) corresponded to 9.2% and 4.3% of their compressive strengths which showed that the assumption of tensile strength of masonry as 10% of compressive strength is an overestimation in

**Table 6** Compressive behaviour for CDP modelling

Mortarless masonry units		Ungouted mortarless masonry		Grouted mortarless masonry	
Stress (MPa)	Crushing strain ( $10^{-3}$ )	Stress (MPa)	Crushing strain ( $10^{-3}$ )	Stress (MPa)	Crushing strain ( $10^{-3}$ )
24.60	0	12.38	0	7.32	0
40.71	0.50	20.68	0.86	8.20	0.15
35.13	0.68	17.79	0.96	9.55	0.37
31.73	0.70	15.90	1.03	10.40	0.52
25.10	0.74	14.92	1.11	11.83	0.95
21.23	0.76		12.20	1.27	
14.54	0.78		11.49	1.34	
10.67	0.79		8.12	1.44	
7.27	0.80				
3.34	0.82				



**Table 7** Tensile behaviour for CDP modelling

Masonry units		UngROUTED walls		Grouted walls	
Stress (MPa)	Cracking strain	Stress (MPa)	Cracking strain	Stress (MPa)	Cracking strain
3.78	0	$\mu f_d$	0	0.53	0

both micro- and macro- modellings. For grouted wallets, its tensile strength can be assumed to be equal to the tensile stress of the grout. However, this recommendation is based on only one grout strength and further investigations with different grout strengths are necessary to confirm this finding. In the case of micro-modelling of ungrouted mortarless masonry walls, an estimate of tensile strength can be assumed to be equal to coefficient of friction times the axial stress at the wall mid-height.

The grouted cores resulted in the average modulus of elasticity of two-stack grouted masonry prism to be 19.6% higher than that of the ungrouted prisms. Due to the lack of mortar to effectively bond the units together, the  $E_m/f_m$  ratio of the ungrouted prisms was significantly lower than observed for mortared masonry. In the case of grouted prisms, the ratio was still lower than observed in mortared masonry but was higher than that of the ungrouted prisms which indicated that the grouts made the prisms relatively stiff.

**Author contributions** Sonam Dorji and Hossein Derakhshan contributed to the research conceptualisation, methodology, investigation and project administration. Formal analysis and the first draft of the manuscript was written by Sonam Dorji. Hossein Derakhshan, David P Thambiratnam supervised the investigation along with the review and editing of the draft manuscript. Tatheer Zahra and Alireza Mohyeddin commented on the draft versions. All authors read and approved the final manuscript.

**Funding** Open Access funding enabled and organized by CAUL and its Member Institutions.

#### Declaration

**Competing interest** The authors declare that there is no competing interest in relation to this work submitted for publication.

**Open Access** This article is licensed under a Creative Commons Attribution 4.0 International License, which

permits use, sharing, adaptation, distribution and reproduction in any medium or format, as long as you give appropriate credit to the original author(s) and the source, provide a link to the Creative Commons licence, and indicate if changes were made. The images or other third party material in this article are included in the article's Creative Commons licence, unless indicated otherwise in a credit line to the material. If material is not included in the article's Creative Commons licence and your intended use is not permitted by statutory regulation or exceeds the permitted use, you will need to obtain permission directly from the copyright holder. To view a copy of this licence, visit <http://creativecommons.org/licenses/by/4.0/>.

#### References

- Huang L, Gao C, Yan L, Li X, Ma G, Wang T (2017) Experimental and analytical modeling of GFRP strengthened grouted mortarless masonry prisms. *Fibers* 5(2):18
- Mohyeddin A, Dorji S, Gad EF, Goldsworthy HM (2017) Inherent limitations and alternative to conventional equivalent strut models for masonry infill-frames. *Eng Struct* 141:666–675
- Sirotti S, Pellicciari M, Di Trapani F, Briseghella B, Carlo Marano G, Nuti C, Tarantino AM (2021) Development and validation of new bouc-wen data-driven hysteresis model for masonry infilled RC frames. *J Eng Mech* 147(11):4021092
- Thamboo JA, Zahra T, Dhanasekar R (2020) Development of design methodology for mortarless masonry system: case study – a resettlement housing colony. *J Build Eng* 27:100973
- Ramamurthy K, Nambiar EKK (2004) Accelerated masonry construction review and future prospects. *Prog Struct Mat Eng* 6(1):1–9
- Hossain MA, Totoev YZ, Masia M (2018) Experimental investigation of semi-interlocking masonry panels under in-plane cyclic displacement
- Dassault Systemes, Abaqus Analysis User's Guide, Providence, RI, 2014.
- Jaafar MS, Thanoon WA, Najm AMS, Abdulkadir MR, Abang Ali AA (2006) Strength correlation between individual block, prism and basic wall panel for load bearing interlocking mortarless hollow block masonry. *Construct Build Mater* 20(7):492–498
- Fortes ES, Parsekian GA, Fonseca FS (2015) Relationship between the compressive strength of concrete masonry and the compressive strength of concrete masonry units. *J Mater Civ Eng* 27(9):4014238



10. ASCE (2017) Seismic evaluation and retrofit of existing buildings, ASCE/SEI 41–17 ed., American Society of Civil Engineers, Reston, VA
11. SA [Standards Australia] (2018) AS 3700:2018 masonry structures. SAI Global Limited, Sydney
12. CEN [Comité Européen de Normalisation] (2005) BS EN 1996–1–1:2005: Eurocode 6. Design of masonry structures. General rules for reinforced and unreinforced masonry structures, British Standards Institute
13. CSA [Canadian Standard Association] (2019) CSA S304:2014:R2019 Design of masonry structures
14. Pauley T, Priestley MN (1992) Seismic design of reinforced concrete and masonry buildings. Wiley, New York
15. Huang L, Liao L, Yan L, Yi H (2014) Compressive strength of double H concrete block masonry prisms. *J Mater Civ Eng* 26(8):6014019
16. Jaafar MS, Alwathaf AH, Thanoon WA, Noorzaei J, Abdulkadir MR (2006) Behaviour of interlocking mortarless block masonry. *Proc Inst Civil Eng Construct Mater* 159(3):111–117
17. Bolhassani M, Hamid AA, Lau ACW, Moon F (2015) Simplified micro modeling of partially grouted masonry assemblages. *Constr Build Mater* 83:159–173
18. Martins ROG, Nalon GH, Alvarenga RDCSSA, Pedroti LG, Ribeiro JCL (2018) Influence of blocks and grout on compressive strength and stiffness of concrete masonry prisms. *Construct Build Mater* 182:233–241
19. Shi T, Zhang X, Hao H, Chen C (2021) Experimental and numerical investigation on the compressive properties of interlocking blocks. *Eng Struct* 228:111561
20. Zahra T, Dhanasekar M (2018) Characterisation and strategies for mitigation of the contact surface unevenness in dry-stack masonry. *Constr Build Mater* 169:612–628
21. Martínez M, Atamturktur S, Ross B, Thompson J (2018) Assessing the compressive behavior of dry-stacked concrete masonry with experimentally informed numerical models. *J Struct Eng* 144(7):4018080
22. Borri A, Castori G, Corradi M, Speranzini E (2011) Shear behavior of unreinforced and reinforced masonry panels subjected to in situ diagonal compression tests. *Constr Build Mater* 25(12):4403–4414
23. Dizhur D, Ingham JM (2013) Diagonal tension strength of vintage unreinforced clay brick masonry wall panels. *Constr Build Mater* 43:418–427
24. Castori G, Corradi M, Speranzini E (2021) Full size testing and detailed micro-modeling of the in-plane behavior of FRM-reinforced masonry. *Constr Build Mater* 299:124276
25. Shabdin M, Zargar M, Attari NKA (2018) Experimental diagonal tension (shear) test of un-reinforced masonry (URM) walls strengthened with textile reinforced mortar (TRM). *Constr Build Mater* 164:704–715
26. Mezrea PE, Ispir M, Balci IA, Bal IE, Ilki A (2021) Diagonal tensile tests on historical brick masonry wallets strengthened with fabric reinforced cementitious mortar. *Structures (Oxford)* 33:935–946
27. Knox CL, Dizhur D, Ingham JM (2018) Experimental study on scale effects in clay brick masonry prisms and wall panels investigating compression and shear related properties. *Constr Build Mater* 163:706–713
28. AM [Adbri Masonry] (2022) Versaloc walling system. <https://www.adbrimasonry.com.au/wp-content/uploads/2021/09/19450-Versaloc-12pp-Brochure-May-2019.pdf>. Accessed 16 Feb, 2022, 2022
29. Dyson JK (2013) Interlocking masonry block. Adbri Masonry, United States Patent, (2013), p. 22.
30. Ltd AB, Report A (2014) Adelaide, South Australia 5000, Adelaide. South Australia 5000:2014
31. ASTM [American Society for Testing and Materials] (2021) C1314 -21 standard test method for compressive strength of masonry prisms. ASTM International, West Conshohocken
32. ASTM [American Society for Testing and Materials] (2021) C140/C140M -21 standard test methods for sampling and testing concrete masonry units and related units. ASTM International, West Conshohocken
33. ASTM [American Society for Testing and Materials] (2020) C1006/C1006M - 20a standard test method for splitting tensile strength of masonry units. ASTM International, West Conshohocken
34. ASTM [American Society for Testing and Materials] (2021) E519/E519M - 21 standard test method for diagonal tension (Shear) in masonry assemblages. ASTM International, West Conshohocken
35. ASTM [American Society for Testing and Materials] (2021) C39/C39M - 21 Standard Test Method for Compressive Strength of Cylindrical Concrete Specimens. ASTM International, West Conshohocken
36. ASTM [American Society for Testing and Materials] (2017) C496/C496 - 17 Standard test method for splitting tensile strength of cylindrical concrete specimens. ASTM International, West Conshohocken
37. Jaafar MS, Thanoon WA, Najm AMS, Abdulkadir MR, Abang Ali AA (2006) Strength correlation between individual block, prism and basic wall panel for load bearing interlocking mortarless hollow block masonry. *Construct Build Mater* 20(7):492–498
38. Balbo JT (2013) Relations between indirect tensile and flexural strengths for dry and plastic concretes. *Revista IBRACON de estruturas e materiais* 6(6):854–874
39. Hossain MA, Totoev YZ, Masia MJ (2016) Friction on mortar-less joints in semi interlocking masonry. pp 1635–1644
40. Martínez M, Atamturktur S (2019) Experimental and numerical evaluation of reinforced dry-stacked concrete masonry walls. *J Build Eng* 22:181–191
41. Mark JT, Sreevalli IY (2021) Numerical study on lateral performance of RC frame with strong masonry infill. *Asian J Civil Eng* 22(3):551–563
42. Zahra T (2017) Strategies for improving the response of drystack masonry to compression. Queensland University of Technology

**Publisher's Note** Springer Nature remains neutral with regard to jurisdictional claims in published maps and institutional affiliations.

